

## NUMERICAL VERIFICATION OF ANALYTICAL SOLUTION FOR AUTOFRETTAGED HIGH-PRESSURE VESSELS

ANDRZEJ TROJNACKI, MACIEJ KRASIŃSKI

*Cracow University of Technology, Department of Mechanical Engineering, Kraków, Poland*

*e-mail: atroj@mech.pk.edu.pl; mkr@mech.pk.edu.pl*

Thick-walled cylinders are widely used in various engineering applications. In an optimal design of pressurized thick-walled cylinders, an increase in the allowable internal pressure can be achieved by an autofrettage process. In the paper, analysis is carried out to develop a procedure in which the autofrettage pressure is determined analytically. The obtained equivalent stress distribution is compared with those of the conventional solid wall and of several multi-layer vessels. The results of the analytical approach are verified by FEM modelling. Tensile tests have been carried out to determine the real mechanical properties of the material of the vessel and to create a material model. The presented example illustrates the advantages of the autofrettage technique.

*Keywords:* autofrettage, optimal solution, finite element verification

### 1. Introduction

Modern power engineering systems and advanced chemical technologies require the use of large thick-walled pressure vessels sustaining the pressure of hundreds MPa. Conventional methods of one thick shell manufacturing (forging or rolling of thick sheets) resulted in technological difficulties and became too expensive. These problems forced engineers to search for new possibilities of increasing load bearing capacity of the vessel. Now, the autofrettage technique is commonly applied to improve the resultant stress distribution and to increase the capacity of the vessel.

A number of contributions to the autofrettage technique have appeared recently. Solutions have been obtained either in an analytical form or with numerical implementations. A procedure for elastic-plastic analysis of a thick-walled cylinder under internal pressure was proposed by Zhao *et al.* (2003). It involves two parametric functions and piecewise linearization of the stress-strain curve. The method provides a general elastic-plastic solution which accounts for the effect of deformed geometry due to high operating pressure. The optimum autofrettage pressure was determined by Ayob and Elbasheer (2007) analytically. A validation by a numerical simulation shows that the analytical approach and numerical results correlate well. Majzoobi *et al.* (2003) used both numerical and experimental techniques for the investigations of the autofrettage process and its influence on the pressure capacity. A finite element analysis was performed by Alegre *et al.* (2006) to obtain the residual stresses after the autofrettage for the vessel made of the material which shows strong Bauschinger's effect. The simulation procedure may be applied for other autofrettage designs that need the Bauschinger effect of the material to be considered. An autofrettage model considering the material strain-hardening relationship and the Bauschinger effect, based on the actual tensile-compressive stress-strain curve of material, plane-strain, and modified yield criterion was proposed by Huang and Cui (2006). The predicted residual stress distributions of autofrettaged tubes from the considered model were compared with the numerical results and the experimental data. The influence of Bauschinger effect and yield criterion on the residual stress was discussed based on the introduced

model. An analytical study of spherical autofrettage-treated pressure vessels, considering the Bauschinger effect was presented by Adibi-Asl and Livieri (2007), where a general analytical solution for stress and strain distributions was proposed for both loading and unloading phases. The optimization procedure, numerical simulation and experiments were employed by Majzoubi and Ghomi (2006) to determine the minimum weight of a compound cylinder for a specific pressure.

Many researchers have focused on methods to extend vessels lifetimes. Fatigue analysis was performed by Koh (2000) to predict the fatigue life of an autofrettaged pressure vessel containing radial holes subjected to cyclic internal pressure. Finite element analysis was used to calculate the residual and operating stress distributions and to determine numerical stress concentration factors at the hole. Analysis of the combined effect of autofrettage and shrink-fit in a multi-layer vessel was carried out by Kumar *et al.* (2011). Thicknesses of layers, autofrettage percentage and radial interference for the shrink-fit were assumed as design variables, whereas hoop stress throughout the thickness was the objective function. Calculation of fatigue life for several cases was studied. The optimum design of a similar 3-layered vessel for maximum fatigue life expectancy under the combined effects of autofrettage and shrink-fit was performed by Jahed *et al.* (2006). The numerical optimization procedure was employed to obtain the optimum size of each layer and to optimize the initial stress distribution. The results showed that with a proper combination of operations, a significant life enhancement could be achieved.

The Tresca-Guest yield condition (the T-G condition) and the Huber-Mises-Hencky yield condition (the H-M-H condition) are used in the present paper to develop a procedure in which the autofrettage pressure is determined analytically. The obtained reduced equivalent stress distribution is compared with distributions for a solid virgin cylinder and for the multi-layer vessel with modified initial stress distribution. A finite element method (FEM) using ANSYS® simulation is carried out on the cylinder to develop a procedure in which the autofrettage process is determined numerically. The real properties of the vessel material are introduced into numerical simulation with the Bauschinger effect implemented. The numerical example illustrates the advantages of the autofrettage technique.

## 2. Analytical solution of the autofrettaged vessel

Theoretical distributions of radial and circumferential stresses in cylindrical vessels within the elastic range must satisfy Lamé's equations (Timoshenko and Goodier, 1951). For this reason, the corresponding distribution of equivalent stress  $\sigma_{eq}$  in the solid wall is precisely determined. In a solid nonpressurized cylinder subjected to the inner operating pressure  $p_{opr}$ , the maximum equivalent stress  $\sigma'_{eq\ max}$  appears at the inner radius while the outer parts of the wall are less loaded. In many industrial applications it is important to decrease the maximum equivalent stress in the wall or to reduce  $\sigma_{eq}$  at the outermost surfaces, which may be additionally subjected to action of aggressive fluids (Fig. 1).

Autofrettage is often used to introduce advantageous residual stresses into thick-walled pressure vessels and to enhance their pressure bearing capacity. In this technique, the vessel is subjected to an internal pressure large enough to cause yielding within the wall near the inner surface. Large scale yielding occurs in the autofrettaged cylinder wall. Upon the release of this pressure, a compressive residual circumferential stress is developed to a certain radial depth at the bore. These residual stresses serve to reduce the stresses obtained as a result of subsequent application of the operating pressure, thus increasing the load bearing capacity.

The degree of autofrettage in the thick-walled cylinder of inner and outer radii  $r_i$  and  $r_o$ , respectively, subjected to the inner autofrettage pressure  $p_a$ , is defined as a junction (limit) radius  $r_j$  of wall thickness occupied by the plastic zone. The radial  $\sigma_r^{el}$  and circumferential  $\sigma_\varphi^{el}$

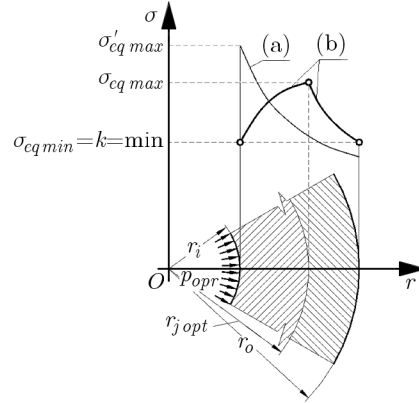


Fig. 1. Condition of minimum equivalent stress  $\sigma_{eq}$  at the junction radius  $r_j$  under the operating pressure  $p_{opr}$ . Distribution of stress  $\sigma_{eq}$ : (a) – in a solid virgin wall, (b) – in the optimum autofrettaged vessel

stresses within the elastic region  $r_j \leq r \leq r_o$  are given in terms of the radius  $r$  by well-known Lamé's formulation

$$\sigma_r^{el} = C_1 - \frac{C_2}{r^2} \quad \sigma_\varphi^{el} = C_1 + \frac{C_2}{r^2} \quad (2.1)$$

In the plastic region  $r_i \leq r \leq r_j$ , theoretical distributions of stress depend on the applied assumptions and the yield theory defining the equivalent stress  $\sigma_{eq}$ . For the elastic-perfectly plastic material model and when the material is incompressible in plastic deformation ( $\nu = 0.5$ ), the more complex H-M-H [ $\Phi_f$ ] yield condition may be linearized for plain strain ( $\varepsilon_z = 0$ ) to that similar to the T-G [ $\tau_{max}$ ] one

$$|\sigma_r^{pl} - \sigma_\varphi^{pl}| = CS_y \quad (2.2)$$

where  $S_y$  stands for the yield stress. The coefficient  $C$  depends on the applied yield theory, and for the T-G yield condition  $C = 1$ , and for the H-M-H yield condition  $C = 2/\sqrt{3}$ . Finally, in both cases, the stresses in the plastic region are expressed by the same equations

$$\sigma_r^{pl} = CS_y \ln\left(\frac{r}{r_o}\right) + C_3 \quad \sigma_\varphi^{pl} = CS_y \left[ \ln\left(\frac{r}{r_o}\right) + 1 \right] + C_3 \quad (2.3)$$

Three constants of integration may be determined from the appropriate boundary conditions and the condition of stress continuity across the elastic-plastic boundary at the junction radius  $r_j$

$$\begin{aligned} r = r_i & \quad \sigma_r^{pl} = -p_a \\ r = r_j & \quad \sigma_r^{pl} = \sigma_r^{el} \quad \sigma_\varphi^{pl} = \sigma_\varphi^{el} \\ r = r_o & \quad \sigma_r^{el} = 0 \end{aligned} \quad (2.4)$$

where the additional fourth condition relates the autofrettage pressure  $p_a$  to the limit radius  $r_j$

$$p_a = CS_y \left[ \ln\left(\frac{r_j}{r_i}\right) + \frac{r_o^2 - r_j^2}{2r_o^2} \right] \quad (2.5)$$

Equation (2.5) is valid for both yield conditions after substituting for  $C$  the appropriate value.

If the autofrettage pressure is removed after a part of the cylinder thickness has become plastic, a residual stress is set up in the wall. Assuming that during unloading the material follows Hooke's law, the residual stress can be easily obtained. The maximum equivalent stress  $\sigma_{eq max}$  in the autofrettaged vessel subjected to the operating pressure  $p_{opr}$  appears at the junction

radius  $r_j$  (Fig. 1) and does not depend on the used yield criterion. If the cylinder is loaded again with the operating pressure, by superposing the residual stresses  $\sigma_r^{res}$  and  $\sigma_\varphi^{res}$  due to autofrettage procedure and stresses  $\sigma_r$  and  $\sigma_\varphi$  produced by the operating pressure, the final equivalent stress distribution in the wall versus radius  $r$  becomes

$$\sigma_{eq}(r) = \frac{1}{C} \left| (\sigma_r + \sigma_r^{res}) - (\sigma_\varphi + \sigma_\varphi^{res}) \right| \quad (2.6)$$

and at the junction radius  $r_j$  takes the form

$$\sigma_{eq}(r_j) = \frac{1}{C} \frac{2r_i^2 r_o^2}{(r_o^2 - r_i^2) r_j^2} [p_{opr} - p_a] + S_y \quad (2.7)$$

Equivalent stress (2.7) reaches the minimum with respect to  $r$  as  $d\sigma_{eq}(r_j)/dr_j = 0$  which leads to the optimum value of the limit radius

$$r_{j\ opt} = r_i \exp\left(\frac{p_{opr}}{C S_y}\right) \quad (2.8)$$

It appears that optimization of the equivalent stress along the vessel wall causes that the difference of equivalent stresses at the outermost radii

$$\begin{aligned} \sigma_{eq}(r_i) &= \frac{1}{C} \frac{2r_o^2}{r_o^2 - r_i^2} [p_{opr} - p_a] + S_y \\ \sigma_{eq}(r_o) &= \frac{2r_j^2}{r_o^2 - r_j^2} \left( \frac{1}{C} p_a - S_y \ln \frac{r_j}{r_i} \right) + \frac{1}{C} \frac{2r_i^2}{r_o^2 - r_i^2} [p_{opr} - p_a] \end{aligned} \quad (2.9)$$

is minimum, and for  $r_j = r_{j\ opt}$  their difference is zero

$$\sigma_{eq} \Big|_{r=r_{j\ opt}}(r_i) = \sigma_{eq} \Big|_{r=r_{j\ opt}}(r_o) = k = \min \quad (2.10)$$

where  $k$  stands for the minimum value of the equivalent stress. Junction radius (2.8) is optimal when for any other value of it an increase in the equivalent stress occurs and the condition of equal and minimum equivalent stresses at the outermost radii under applied operating pressure is disturbed. The autofrettage pressure which is necessary to obtain the optimum limit radius, (2.8), may be determined from Eq. (2.5). In the autofrettaged vessel, the maximum strength  $\sigma_{eq\ max}$  under the operating pressure  $p_{opr}$  appears at the junction radius. Application the optimum autofrettage pressure and partial yielding of the wall to the optimum junction radius causes minimum equivalent stress under the operating pressure and equal and minimum values of the equivalent stress at the outermost radii. The maximum operating pressure is equal to the autofrettage pressure  $p_{max} = p_{a\ opt}$ . Under this pressure, full yielding of the vessel wall in the range  $r < r_{j\ opt}$  appears again and the decay of the equivalent stress in the range  $r_{j\ opt} \leq r \leq r_o$ .

The maximum autofrettage pressure  $p_{a\ extr}$  corresponds to the internal pressure required for the wall thickness of cylinder to yield completely  $r_{j\ extr} = r_o$ . Such a cylinder may be subjected to the maximum operating pressure  $p_{extr} = p_{a\ extr}$ .

### 3. Finite element modelling of the autofrettaged vessel

The autofrettage process has been simulated by the finite element method (FEM) making use of elastic-plastic analysis. Special crude alloy steel 16Mo3 (1.5415) according to PN-EN 10028-2: 2010 has been applied for the vessel wall. This material is assigned to high-temperature applications and is often used in the high-pressure technology. Actual mechanical properties of this

material have been determined in tensile tests. A set of cylindrical specimens has been cut from a segment of a tube in the circumferential direction. The specific values of material data have been calculated as arithmetical averages of 7 tests: ultimate strength  $S_{ut} = 518.43$  MPa, yield limit  $S_y = 317.29$  MPa, maximum strain  $\varepsilon_{ut} = 0.1750$  and plastic strain  $\varepsilon_{pl} = 0.0127$ . They are defined in Fig. 2 together with the elastic strain which for Young's modulus  $E = 2.1 \cdot 10^5$  MPa adopted in the elastic range becomes  $\varepsilon_{el} = 0.0015$ .

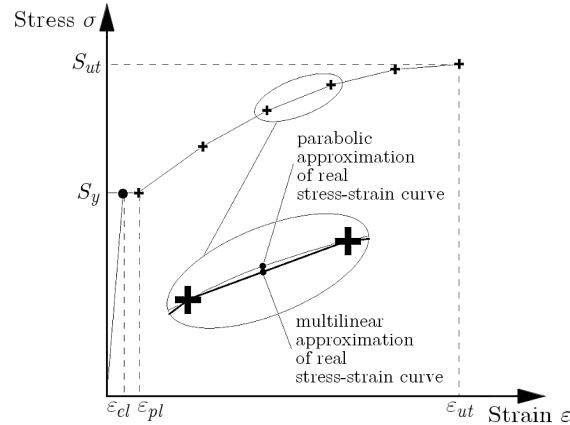


Fig. 2. Parabolic and segmental approximation of the real stress-strain curve (in the stretched scale)

The shape of experimental stress-strain curves  $\sigma = f(\varepsilon)$  suggests parabolic approximation beyond the yield limit. The parabola containing the point of coordinates  $\varepsilon_{pl}$ ,  $S_y$  and reaching the maximum value at the point  $\varepsilon_{ut}$ ,  $S_{ut}$  (Fig. 2) was applied to describe the tensile behaviour of material. For the numerical calculations the parabola was replaced by five segments of different slopes but of equal length in the orthogonal projection at the  $\varepsilon$  axis. Such an approximation enables direct introduction of the nonlinear material properties in the software module ANSYS® which was used in the paper.

Moreover, it was assumed that the relationship between the equivalent stress (stress intensity)  $\sigma_{eq}$  and equivalent strain (strain intensity)  $\varepsilon_{eq}$  under complex stress states  $\sigma_{eq} = f(\varepsilon_{eq})$  was the same as the stress-strain relationship under uniaxial tensile loading. The stress intensity was derived from the Huber-Mises-Hencky yield criterion and the strain intensity was defined (Życzkowski, 1981) as

$$\varepsilon_{eq} = \frac{2}{\sqrt{3}} \sqrt{(\varepsilon_r - \varepsilon_\varphi)^2 + (\varepsilon_\varphi - \varepsilon_z)^2 + (\varepsilon_z - \varepsilon_r)^2} \quad (3.1)$$

where  $\varepsilon_r$ ,  $\varepsilon_\varphi$  and  $\varepsilon_z$  are principal strains at a certain point of the cross-section.

The finite element calculations were carried out on the assumption of plain strain which seems justified as the cylindrical parts of the vessels are usually of considerable length. The material of the vessel was described by multi-linear kinematic strain hardening with the Baushinger effect included.

FEM modelling of the vessel wall geometry is simplified because of the axial symmetry. The numerical model of the wall was built of layers (rectangular slices) of the assumed radii divided into higher order finite elements PLANE183 adapted to the axial symmetry. The size of quadratic 8-node finite elements of 0.4 mm creates the mesh of sufficient density as an increase of the density in five times produces the difference in the equivalent stress less than 0.4%. A typical finite element mesh with boundary conditions applied is presented in Fig. 3.

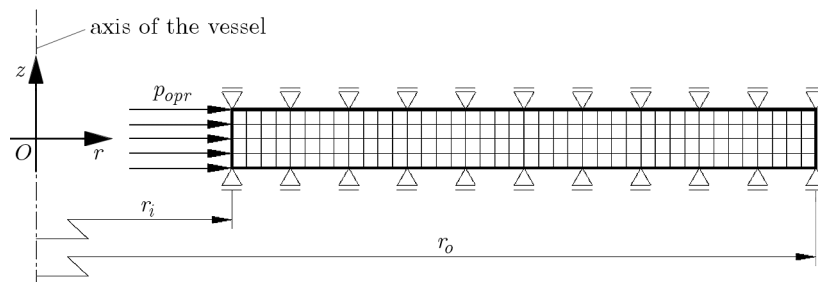


Fig. 3. Computational model of the vessel, mesh of finite elements and illustration of introduced boundary conditions (not to scale)

#### 4. Numerical example

The detailed analytical and numerical calculations were carried out for a cylinder of the outer diameter  $2r_o = 800$  mm subjected to internal pressure. The thickness of the wall was  $t_o = 200$  mm. The vessel was made of material 16Mo3 with the experimentally confirmed yield point  $S_y = 317.29$  MPa. The vessel was designed for the operating pressure  $p_{opr}$  under which the equivalent stress reaches the yield limit  $S_y$  at a certain point of the wall. The pressure  $p_{opr}$  derived from the T-G  $[\tau_{max}]$  yield criterion is  $p_{opr}^T = 118.98$  MPa and that based on the H-M-H  $[\Phi_f]$  yield criterion is  $p_{opr}^H = 137.39$  MPa.

On the applied assumptions, the T-G and H-M-H yield conditions may be expressed by the same equation (2.2) and, therefore, both criteria lead to similar results of the autofrettage. For this reason, the distributions of equivalent stress at some characteristic radii versus the junction radius  $r_j$  for the vessel subjected to the operating pressure  $p_{opr}^T$  or  $p_{opr}^H$ , respectively, are the same (Fig. 4). The only difference is in relation (2.5) describing the autofrettage pressure  $p_a$  versus the autofrettage radius  $r_j$ .

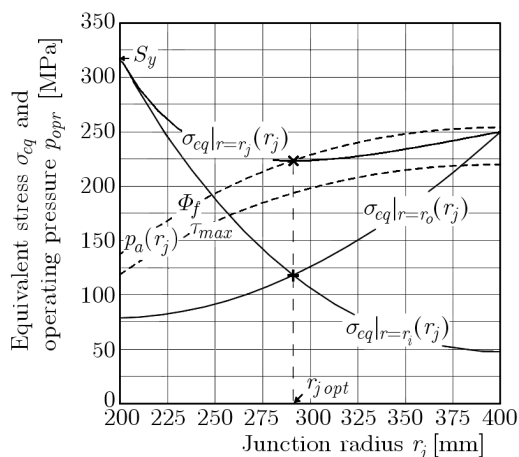


Fig. 4. Equivalent stress  $\sigma_{eq}$  under pressure  $p_{opr}^T$  or  $p_{opr}^H$  at the radii:  $r_j$ ,  $r_i$  and  $r_o$ , respectively, and the autofrettage pressure  $p_a$  versus junction radius  $r_j$

The optimum autofrettage radius is the same  $r_{j,opt} = 290.99$  mm for both criteria, but the autofrettage pressure is different. For the T-G yield condition,  $p_{a,opt}^T = 193.66$  MPa and for the H-M-H yield condition,  $p_{a,opt}^H = 223.63$  MPa. Under the pressure  $p_{opr}^T$  or  $p_{opr}^H$ , the equivalent stress at the outer radii is the same and reaches minimum  $\sigma_{eq}(r_i) = \sigma_{eq}(r_o) = 118.14$  MPa. The maximum equivalent stress in the considered vessel occurs at the junction radius  $\sigma_{eq}(r_{j,opt}) = 223.22$  MPa. The distributions of equivalent stress at the outermost radii  $\sigma_{eq}|_{r=r_i}$  and  $\sigma_{eq}|_{r=r_o}$  are plotted in Fig. 4 versus the junction radius  $r_j$  (solid fine lines) as well as the

autofrettage pressure versus the corresponding junction radius (dashed lines). Any other modification of the residual stress resulting in the junction radius different from  $r_{j\ opt}$  causes an increase in the maximum equivalent stress  $\sigma_{eq}(r_{j\ opt})$  which can be seen in Fig. 4 (bold solid line).

Analytical results for the autofrettaged vessel are gathered in Table 1. The calculations were carried out for the vessel autofrettaged to the optimum limit radius  $r_{j\ opt}$  and to the maximum limit radius  $r_{j\ extr} = 400$  mm. In both cases, the vessel was subjected first to the pressure  $p_{opr}$  ( $p_{opr}^T$  or  $p_{opr}^H$ ) and then to the maximum pressure ( $p_{a\ opt}$  for  $r_{j\ opt}$  or  $p_{a\ extr}$  for  $r_{j\ extr}$ ). The relative decrease of the maximum equivalent stress  $\Delta\sigma_{eq}$  with respect to the solid wall was determined in the first case and the relative increase of the load bearing capacity  $\Delta p_{max}$  was determined in the second case. The total yielding of the wall calculated analytically based on the Tresca-Guest yield criterion occurs under the autofrettage pressure  $p_{a\ extr}^T = 219.93$  MPa and this is the maximum operating pressure which may be applied to the vessel. The calculations carried out for the Huber-Mises-Hencky yield condition give  $p_{a\ extr}^H = 253.95$  MPa.

**Table 1.** Decrease of the equivalent stress and increase of the load capacity for several types of vessels

Type of the wall	Number of layers or junction radius $r_j$ [mm]	Calculations	Under operating pressure		Under maximum pressure	
			Maximum strength $\sigma_{eq}$ [MPa]	Decrease of strength $\Delta\sigma_{eq}$ [%]	Maximum capacity $p_{max}$ [MPa]	Increase of capacity $\Delta p$ [%]
Layered optim. under $p_{opr}$	2 layers	analytical	239.63	24.48	171.02	24.48
	25 layers	analytical	176.65	44.33	207.71	51.18
Autofrettaged to $r_{j\ opt}$	$r_{j\ opt} = 290.99$	analytical	223.22	29.65	223.63	62.77
	$r_{j\ opt} = 291.60$	FEM	223.16	29.67	222.51	62.24
Layered optim. under $p_{max}$	2 layers	analytical	271.59	14.40	181.91	32.40
	25 layers	analytical	251.54	20.72	246.77	79.61
Autofrettaged to $r_{j\ extr}$	$r_{j\ extr} = 400$	analytical	249.99	21.21	253.95	84.84
	$r_{j\ extr} = 400^{1)}$	FEM	248.56	21.66	251.38	83.29
	$r_{j\ extr} = 400^{2)}$	FEM	235.51	25.77	266.79	94.52
	$r_{j\ extr} = 400^{3)}$	FEM	251.46	20.75	311.38	127.04

- 1) autofrettage pressure  $p_{a\ extr\ 1}^{FEM} = 251.38$  MPa,  
strain intensity  $\varepsilon_{eq}(r_i) = 0.0067$ ,  $\varepsilon_{eq}(r_o) = 0.0015$
- 2) autofrettage pressure  $p_{a\ extr\ 3}^{FEM} = 266.79$  MPa,  
strain intensity  $\varepsilon_{eq}(r_i) = 0.0501$ ,  $\varepsilon_{eq}(r_o) = 0.0127$
- 3) autofrettage pressure  $p_{a\ lim}^{FEM} = 311.38$  MPa,  
strain intensity  $\varepsilon_{eq}(r_i) = 0.1750$ ,  $\varepsilon_{eq}(r_o) = 0.0488$

The distributions of equivalent stress  $\sigma_{eq}$  versus the radius  $r$  for the vessels autofrettaged to the radius  $r_{j\ opt}$  (dashed lines) and to the radius  $r_{j\ extr}$  (solid lines) under the pressure  $p_{opr}$  (fine lines) and under the pressure  $p_{a\ opt}$  or  $p_{a\ extr}$  (bold lines) are presented in Fig. 5. The dotted line corresponds to the solid non-pressurized wall subjected to the maximum in this case pressure  $p_{opr} = 137.39$  MPa.

The analytical solution of the autofrettaged vessel was compared with the analytical results obtained for the optimum shrink-fit multi-layer vessels (Kraśiński *et al.*, 2013). The results are gathered in Table 1. The H-M-H yield criterion was applied to solve the wall composed of 2 layers and of 25 layers of the same thickness. The layered vessels were designed on the assumption of equal equivalent stress at the inner surfaces of layers under the pressure  $p_{opr} = 137.39$  MPa. The distributions of the equivalent stress versus the radius  $r$  are plotted in Fig. 6 (solid fine lines) and

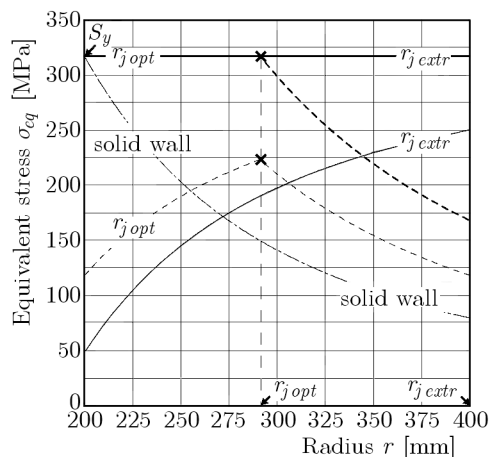


Fig. 5. Equivalent stress  $\sigma_{eq}$  of the wall autofrettaged to the radii:  $r_{j\ opt}$  or  $r_{j\ extr}$ , respectively, versus radius  $r$ . Fine lines – under the pressure  $p_{opr}$ , bold lines – under the maximum pressure  $p_{a\ opt}$  or  $p_{a\ extr}$

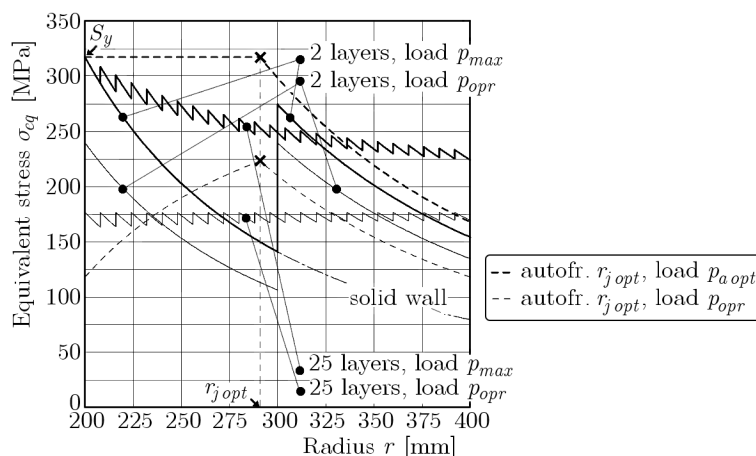


Fig. 6. Distribution of  $\sigma_{eq}$  versus radius  $r$  for the vessel autofrettaged to  $r_{j\ opt}$  and for the layered vessel with  $\sigma_{eq}$  equalized for pressure  $p_{opr} = 137.39$  MPa

may be compared with the distribution for the vessel autofrettaged to the junction radius  $r_{j\ opt}$  (dashed fine lines). Bold lines correspond to the equivalent stresses which appear in these vessels under the maximum pressure  $p_{max}$  for the shrink-fit vessels or  $p_{a\ opt}$  for the autofrettaged vessel. In this case, the maximum pressure  $p_{max}$  for the multi-layer vessels is the loading for which the yield limit  $S_y$  is first reached at the inner surface of radius  $r_i$ . Variations in the equivalent stress across the wall determined for the multi-layer vessels under the pressure  $p_{max}$  which leads in this case to the condition of maximum strength  $\sigma_{eq}$  equal to the yield limit  $S_y$  at the inner surfaces of all layers are presented in Fig. 7. They are compared with the distributions obtained for the vessel autofrettaged to the radius  $r_{j\ extr}$ .

The residual radial stresses  $\sigma_r^{res}$  calculated analytically for the autofrettaged vessel are illustrated graphically in Fig. 8 together with the interlayer initial compressive stresses  $q_{i\ opt}$  which must be introduced into the layered vessel wall in order to equalize the equivalent stress at the inner surfaces of layers under the operating pressure. The autofrettage process was solved using the Huber-Mises-Hencky yield theory. The residual stress which occurs in the vessel wall autofrettaged to the optimum junction radius  $r_{j\ opt}$  can be compared with the interlayer stresses  $q_{i\ opt}$  which causes the same and equal equivalent stress under the operating pressure  $p_{opr} = 137.39$  MPa. The residual radial stress which appears in the vessel wall autofrettaged

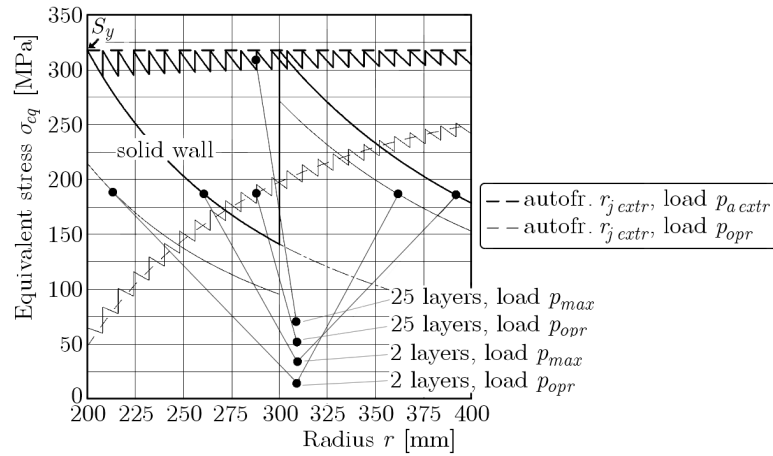


Fig. 7. Distribution of  $\sigma_{eq}$  versus radius  $r$  for the vessel autofrettaged to  $r_{j\,extr}$  and for the layered vessel with  $\sigma_{eq}$  equalized to the maximum value  $S_y$

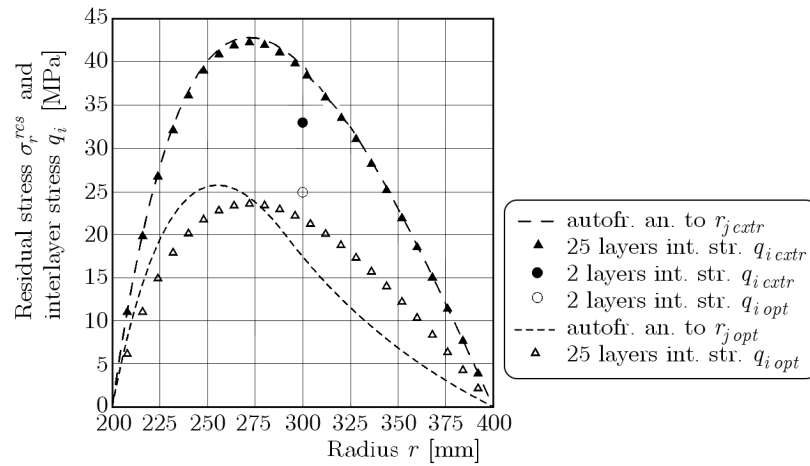


Fig. 8. Dashed lines – distributions of radial residual stress  $\sigma_r^{res}$  for the vessels autofrettaged to  $r_{j\,opt}$  and to  $r_{j\,extr}$ , respectively. Discrete distributions refer to the initial interlayer compressive stresses in layered walls: 2-layer:  $\bullet$  –  $q_{i\,extr}$ ,  $\circ$  –  $q_{i\,opt}$ , and 25-layer:  $\blacktriangle$  –  $q_{i\,extr}$ ,  $\triangle$  –  $q_{i\,opt}$

to the maximum radius  $r_{j\,extr} = 400$  mm may be compared with the interlayer stresses  $q_{i\,extr}$ , which ensures the maximum equivalent stress  $\sigma_{eq}$  equal to  $S_y$  under the maximum operating pressure  $p_{max}$ .

The autofrettage process was modelled by applying pressure to the inner surface of the vessel, removing it and then calculating the residual stress field, followed by reloading with the operating pressure. The finite element procedure was carried out first on the vessel autofrettaged with the pressure  $p_{a\,opt}^{FEM} = 222.51$  MPa which, under the assumed operating pressure  $p_{opr}^{FEM} = 137.15$  MPa, ensures the equality of the equivalent stress at the outermost radii  $\sigma_{eq}(r_i) = \sigma_{eq}(r_o) = 121.16$  MPa and at the limit radius produces  $\sigma_{eq}(r_{j\,opt}) = 223.16$  MPa. The maximum pressure which may be applied to this vessel is the autofrettage pressure  $p_{a\,opt}^{FEM}$ . The results presented in Table 1 are closed to those predicted by the analytical approach. The optimum radius  $r_{j\,opt}$  of the elastic-plastic junction in the autofrettaged cylinder derived for the elastic-perfectly plastic material does not differ significantly compared with that obtained using an elastic-plastic with a strain hardening material model. The reason is that the maximum strain intensity which appears at the inner radius  $\varepsilon_{eq}(r_i) = 0.0035$  is less than  $\varepsilon_{pl} = 0.0127$ . Accordingly, only the first two rectilinear fragments of the stress-strain relationship were used in the numerical procedure, likewise in analytical calculations. A certain small discrepancy is caused by numerical errors.

Moreover, the FEM and analytical results coincide on the assumption that the junction radius  $r_{j\text{extr}} = 400$  mm is achieved when the equivalent stress reaches the first the yield limit  $S_y$  there. Such a situation occurs under the autofrettage pressure  $p_{a\text{extr}1}^{\text{FEM}} = 251.38$  MPa. The strain hardening of the material was not engaged in the numerical procedure. While the strain intensity at the outer radius  $\varepsilon_{eq}(r_o) = 0.0015$  is associated with the yield limit  $S_y$ , the strain intensity at the inner radius  $\varepsilon_{eq}(r_i) = 0.0067$  is less than  $\varepsilon_{pl} = 0.0127$  and corresponds to the  $S_y$  too. The strain hardening has no influence on the numerical solution even for the autofrettage pressure  $p_{a\text{extr}2}^{\text{FEM}} = 252.30$  MPa under which the strain intensity at the inner radius  $\varepsilon_{eq}(r_i) = \varepsilon_{pl} = 0.0127$  because at the outer radius there is still  $\varepsilon_{eq}(r_o) = 0.0030 < \varepsilon_{pl}$ .

The influence of the parabolic part of the stress-strain curve on the finite element solution is revealed only for the autofrettage pressure greater than  $p_a > p_{a\text{extr}2}^{\text{FEM}}$ . A distinct effect is observed on the assumption that the strain intensity at the outer radius reaches  $\varepsilon_{eq}(r_o) = 0.0127 = \varepsilon_{pl}$ , which occurs for the autofrettage pressure  $p_{a\text{extr}3}^{\text{FEM}} = 266.79$  MPa. The strain intensity at the inner radius becomes  $\varepsilon_{eq}(r_i) = 0.0501 > \varepsilon_{pl}$ . Examination of the equivalent stress distributions depicted in Fig. 9 leads to the conclusion that in the whole cross-section, the equivalent stress is beyond the yield limit  $S_y$ , however, at the same time  $p_{a\text{extr}3}^{\text{FEM}} < p_{a\text{lim}}^{\text{FEM}} = 311.38$  MPa. The equivalent stress at the inner radius of the cylinder subjected to  $p_{a\text{lim}}^{\text{FEM}}$  reaches the ultimate tensile strength  $\sigma_{eq}(r_i) = S_{ut} = 518.43$  MPa and may be considered as the maximum pressure for the vessel. The results for a vessel autofrettaged with pressures  $p_{a\text{opt}}^{\text{FEM}}$  and  $p_{a\text{extr}1}^{\text{FEM}}$  are additionally repeated in Fig. 9. Like in Figs. 6 and 7, fine lines refer to the distributions under the operating pressure  $p_{opr}$ . Bold lines in Fig. 9 correspond to the equivalent stress distributions of the autofrettaged cylinder subjected in each case to the maximum pressure (equal to the autofrettage pressure). The numerical results for both considered cases are summarized in Table 1.

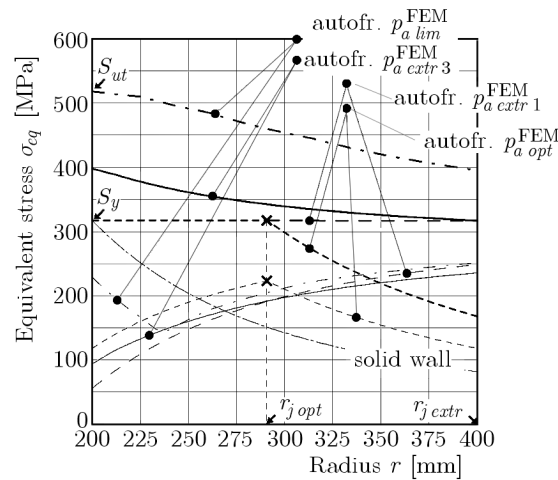


Fig. 9. Equivalent stress  $\sigma_{eq}$  versus radius  $r$  under pressure  $p_{opr}$  (fine lines) and under maximum pressure (bold lines) for the vessel autofrettaged to the radii:  $r_{j\text{opt}}$  and  $r_{j\text{extr}}$ , respectively

The equivalent stress distribution under the operating pressure  $p_{opr}$  for the cylinder subjected to the autofrettage pressure  $p_{a\text{lim}}^{\text{FEM}}$  is of particular interest. The increase of the radius, starting from  $r_i$ , is at the beginning associated with the decrease of the stress. In the vicinity of the radius  $r = 236.80$  mm, there is a marked increase of the stress which continues until the outer radius  $r_o$  is reached. It is caused by the distribution of circumferential residual stress which changes the sign from minus to plus.

The distributions of radial residual stress  $\sigma_r^{\text{res}}$  after the autofrettage pressure is removed for all cases considered in the finite element procedure are plotted in Fig. 10. It can be seen that despite the increase of the autofrettage pressure  $p_{a\text{lim}}^{\text{FEM}} > p_{a\text{extr}3}^{\text{FEM}} > p_{a\text{extr}1}^{\text{FEM}}$ , the corresponding distributions of residual radial stress tend to decrease. Moreover, the relative decrease of the

maximum values of  $\sigma_r^{res}$  (15.36% and 32.27%) is greater than the relative increase of the autofrettage pressure  $p_a$  (6.13% and 23.87%). Such a relation may occur as the strain hardening was taken into account in the FEM procedure.

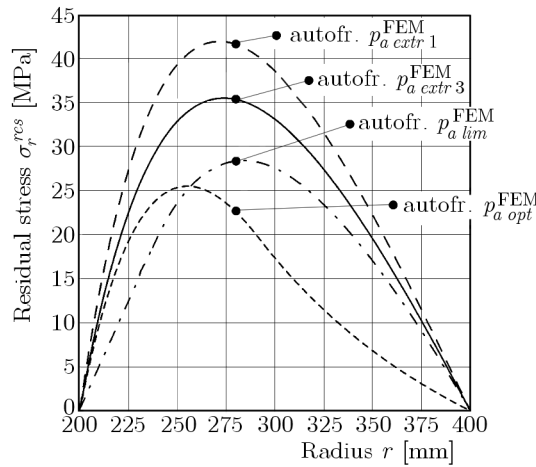


Fig. 10. Distributions of radial residual stress  $\sigma_r^{res}$  versus radius  $r$  for vessels autofrettaged to the radii:  $r_{j\ opt}$  and  $r_{j\ extr}$ , respectively

The finite element calculations were carried out for the 16Mo3 material for which a stress-strain approximation was created using the data derived from the tensile tests. In particular, this steel seems to be a good material to fabricate thick-walled cylinders which are to be subjected to the autofrettage process, mainly on account of a high ultimate strain value  $\varepsilon_{ut}$  and a considerable difference between  $\varepsilon_{el}$  and  $\varepsilon_{pl}$ . This material is plastic enough and able to withstand large deformations, which is the key requirement in the autofrettage process. Owing to the latter property, the favourable effects of strain hardening on the vessel performance manifest at high autofrettage pressures exceeding  $p_{a\ extr\ 2}^{FEM} = 252.30$  MPa.

The horizontal junction segment (plastic plateau) of the stress-strain curve approximation (Fig. 2) is called the perfectly plastic flow and corresponds to the yield point  $S_y$ . The influence of the length of the plastic plateau on some selected strength parameters is shown in Fig. 11. The total length of the plateau was subdivided into five segments of equal length  $\Delta\varepsilon = 0.0022$ , and FEM calculations were carried out for the appropriate five approximations of the stress-strain curve. The parabolic part of the approximation had a maximum (as previously) at the point with the coordinates  $\varepsilon_{ut}$ ,  $S_{ut}$  but in each case the parabola was passing through a different point with coordinates depending on the plastic plateau division. The results are summarized in Fig. 11 where the bold solid line represents the autofrettage pressure  $p_{a\ extr\ 3}^{FEM}$  which increases with the increase in the plastic plateau length. The fine solid line corresponds to the operating pressure  $p_{opr}$  under which the equivalent stress at the outermost radii was set equal to the values indicated in Fig. 11 by the dashed line. It should be noted that all considered parameters of the autofrettaged vessel vary linearly versus the length of the plastic plateau. It appears that an increase in length of the plastic plateau, from zero to its maximum value, gives rise to a slight increase (by 4.77%) in the autofrettage pressure and to a significant reduction (by 11.40%) of the operating pressure  $p_{opr}$  equalizing the equivalent stress at the outermost radii.

The autofrettage has obvious advantages when applied to thick walls characterized by a high thickness coefficient defined as  $\beta = r_o/r_i$ . Several strength parameters of the vessel autofrettaged with the optimum pressure versus the coefficient  $\beta$  are presented in Fig. 12. The examination of these relationships leads to the conclusion that a decrease in the coefficient  $\beta$  in 40% gives rise to reduction of the maximum pressure  $p_{a\ extr}$  by 73.70%, while the maximum equivalent stress at the junction radius increases by 22.48%.

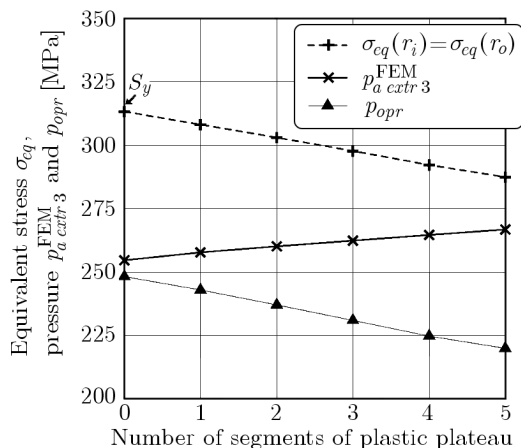


Fig. 11. Autofrettage pressure  $p_{a\ cxtr\ 3}^{FEM}$  and the pressure  $p_{opr}$  equalizing the equivalent stress at the outermost radii (along dashed line) versus the length of the plastic plateau

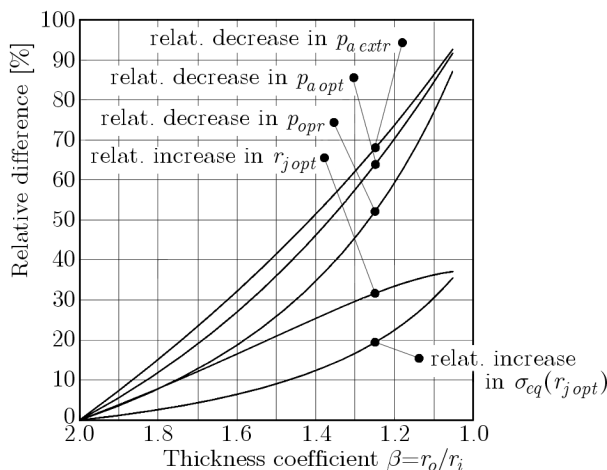


Fig. 12. Some characteristic parameters of the autofrettaged vessel versus the thickness coefficient  $\beta$

### 5. Final remarks

The presented investigations confirm the advantages of the autofrettage technique applied to thick-walled, high-pressure vessels. The advantages were demonstrated using an example of a cylindrical vessel with the outer diameter of 800 mm regarded to be the maximum value with respect to costs for the solid vessel. For vessels with greater outer diameters, a better solution is a layered wall composed of thin layers either shrink-fitted, bent along the screw or spiral line or fabricated using the Smith technology. The maximum value of the thickness coefficient  $\beta = 2.00$  was assumed which is admissible in the strength analysis of the pressure vessels under the regulations of the Polish Office of Technical Inspection (OTI). The vessel is made of ductile 16Mo3 steel which is appropriate for autofrettage processes because of its mechanical behaviour, in particular of the high value of the ultimate strain  $\epsilon_{ut}$ . The analytical well-known approach based on Lamé’s solution reveals that the autofrettage optimum pressure results in a 30% decrease of the equivalent stress under operating pressure. However, the strength capacity of this vessel increases by 63% with respect to the solid virgin wall. Even greater spectacular strength effect may be achieved for the cylinder autofrettaged across its wall giving rise to the load bearing capacity by 85%.

Residual stresses can be also generated by introducing the interlayer interference fit into the multi-layer cylinder. The advantages of autofrettage applied to the solid wall were compared with

the results obtained for the optimum designed layered vessels. The wall composed of 2 layers exhibits a 24% decrease of the equivalent stress under the operating pressure, and this result is similar to that obtained for the solid wall subjected to optimum autofrettage, but the appropriate increase of the load-bearing capacity by 25% is even less. The strength possibilities of the wall made of a large number thin layers may be utilised in a larger degree. The results of analytical calculations compiled in Table 1 suggest that the advantages of layered wall composed of 25 layers are comparable to those of the autofrettaged wall.

The results of FEM simulation and their comparison with the analytical approach is of particular importance. Since the vessel wall is made of a typical material used in the autofrettage technology, the strain hardening effect occurring beyond the yield limit cannot be utilised. As the plastic plateau is of considerable length, the results of FEM calculations for autofrettaged vessel under the optimum and maximum pressures coincide (within the admissible error limits) with the analytical results. Major differences are revealed for a cylinder autofrettaged with a pressure which produces the equivalent stress equal to the ultimate stress at the inner surface. Such a vessel exhibits the maximum possible load carrying capacity for the assumed dimensions and the material which exceeds by 127% the pressure that can be withstood by a solid wall of the same dimensions and material.

In conclusion, it should be mentioned that the well-designed autofrettage technique has obvious advantages over other technologies of thick-walled vessels, in particular over multi-layer technologies. The design is material-saving and cost-effective. In the case of shrink-fit cylinders, care must be taken to ensure precise fits between the layers, which presents serious difficulties when handling elements of considerable length and diameters. Moreover, the shrink-fit cylinders have to be heated (or cooled down), which requires large furnace installations. The Smith method utilises the thermal shrinkage of the longitudinal welds whose magnitude can be only approximately determined. In the light of the current expertise in the field of forging machines (presses and rollers), only high-efficiency pumps are required in fabrication of a typical thick-walled autofrettaged vessel.

## References

1. ADIBI-ASL R., LIVIERI P., 2007, Analytical approach in autofrettaged spherical pressure vessels considering the Bauschinger effect, *Transactions of the ASME, Journal of Pressure Vessel Technology*, **129**, 411-419
2. ALEGRE J.M., BRAVO P., PRECIADO M., 2006, Design of an autofrettaged high-pressure vessel, considering the Bauschinger effect, *Proceedings of the Institution of Mechanical Engineers, Part E*, **220**, 1, 7-16
3. AYOB A., ELBASHEER M.K., 2007, Optimum autofrettage pressure in thick cylinders, *Jurnal Mekanikal*, **24**, 1-14
4. HUANG X.P., CUI W.C., 2006, Effect of Bauschinger effect and yield criterion on residual stress distribution of autofrettaged tube, *Transactions of the ASME, Journal of Pressure Vessel Technology*, **128**, 212-216
5. JAHED H., FARSHI B., KARIMI M., 2006, Optimum autofrettage and shrink-fit combination in multi-layer cylinders, *Transactions of the ASME, Journal of Pressure Vessel Technology*, **128**, 196-200
6. KOH S.K., 2000, Fatigue analysis of autofrettaged pressure vessels with radial holes, *International Journal of Fatigue*, **22**, 8, 717-726
7. KRASIŃSKI M., STODULSKI M., TROJNACKI A., 2013, Stress modification in multi-layer walls of expanded pressure vessels, *Key Engineering Materials*, **542**, 81-95

8. KUMAR N., MONDAL S.C., MANDAL D.K., ACHARYAA S.K., 2011, Optimum autofrettage pressure and shrink-fit combination for minimum stress in multilayer pressure vessel, *International Journal of Engineering, Science and Technology*, **3**, 5, 4020-4030
9. MAJZOABI G.H., FARRAHI G.H., MAHMOUDI A.H., 2003, A finite element simulation and an experimental study of autofrettage for strain hardened thick-walled cylinders, *Materials Science and Engineering*, **359**, 1/2, 326-331
10. MAJZOABI G.H., GHOMI A., 2006, Optimisation of autofrettage in thick-walled cylinders, *Journal of Achievements in Materials and Manufacturing Engineering*, **16**, 1/2, 124-131
11. TIMOSHENKO S., GOODIER J.N., 1951, *Theory of elasticity*, McGraw-Hill Book Company, Inc. N. York, Toronto, London
12. ZHAO W., SESHADRI R., DUBEY R.N., 2003, On thick-walled cylinder under internal pressure, *Transactions of the ASME, Journal of Pressure Vessel Technology*, **125**, 267-273
13. ŻYCKOWSKI M. (EDIT.), 1981, *Combined Loadings in the Theory of Plasticity*, Polish Sci. Publ., Warszawa

*Manuscript received December 6, 2013; accepted for print February 20, 2014*